Classification of Two-Phase Flow Instability by Density Wave Oscillation Model

Kenji FUKUDA,

*Faculty of Engineering, Kyushu University**

Tetsuo KOBORI

*O-arai Engineering Center, Power Reactor and Nuclear Fuel Development Corporation***

Received August 4, 1978
Revised November 1, 1978

An analysis shows that hydrodynamic instabilities of two-phase flow are classified into at least eight types. Three of them are roughly classified into the static or the Ledinegg instability, and other five of them into the dynamic or the density wave instability.

Two typical types of instabilities are observed in our experiment, in each type different pressure drop term: gravitational or frictional pressure drop of two-phase flow is found to be the governing term.

Classification method of instabilities and its applications are presented.

KEYWORDS: hydrodynamic instability, two phase flow, density wave oscillation, Ledinegg instability, oscillation, stability map, classification, Nyquist diagram, transfer function

I. INTRODUCTION

Hydrodynamic instability of two-phase flow is of particular interest and many studies[1]~[12] have been already conducted.

It is of great importance, in this problem, to classify the apparently much varied phenomena into basic types, and some attempts have been made[3]~[6]. The most important types of instabilities seems to be the Ledinegg instability[11] and the density wave instability[10], which Boure[4] empirically classified into static and dynamic instabilities respectively. However these classifications are rather rough because they can not give hints concerning the cause of the instability or the technical measure to prevent it. Sumida *et al.*[3] made an analytical study and classified the instabilities into three types. The structure of the instability became much clear in their analysis, however, it still remains to gain more prospective insight into the problem by using a simpler model to avoid a complexity of the resulting equations.

In another paper[7], we have shown our experimental results which can be classified into two types of instabilities both being classified into the density wave instability. One has a characteristic feature that it occurs at a nearly zero exit steam quality condition (Type I), and another occurs at high steam quality (Type II).

An analysis[7] has shown that the gravitational pressure drop in the unheated riser

* *Hakozaki, Higashi-ku, Fukuoka 812.*
** *O-arai-machi, Ibaraki-ken 311-13.*

section plays a dominant role in Type I instability, while the frictional pressure drop is dominant in Type II instability. It is worth noting that this kind of classification into the "Types", in which different pressure drop term is the governing factor in each "Type", implies the existance of other "Types" of instabilities than above two "Types".

In this paper experimental results both under natural and forced circulation conditions in two parallel channels are described, in which attempts were made to examine the role of adiabatic riser pipings. Then the analytical method for the classification of hydrodynamic instabilities is offered and applied to some experimental results.

II. EXPERIMENTS

1. Experimental Apparatus and Method

Experiments were performed by using the 14 MW heat transfer loop which is installed at O'arai Engineering Center, Power Reactor and Nuclear Fuel Development Corporation (PNC), Japan. Flow diagram of this loop is shown in **Fig. 1**. The loop consists of a steam drum, subcooler, preheater, pump, two parallel vertical heated sections and inlet and riser pipings.

In forced circulation tests the pump was operated to keep the total flow constant, while it was bypassed in natural circulation tests.

Two similar vertical heaters, which simulate reactor fuel clusters, were heated electrically. Effective heated length, equivalent diameter and flow area are 3.7 m, 9.71 mm, 46.86 cm^2 respectively and a cluster consists of 28 rods. **Figure 2** describes the pipings of unheated risers. Most experiments were carried out by using the risers (A), and shorter riser pipings (B) were used in the additional tests. This variety of piping and the riser joint valve set in the halfway of the pipe line (A) were employed to examine the role of risers.

Experiments were carried out by increasing heating power input under constant system pressure and inlet temperature conditions. Inlet throttlings in natural circulation tests, or total flow rate (a sum of channel flow rates) in forced circulation tests was also kept constant. Experimental

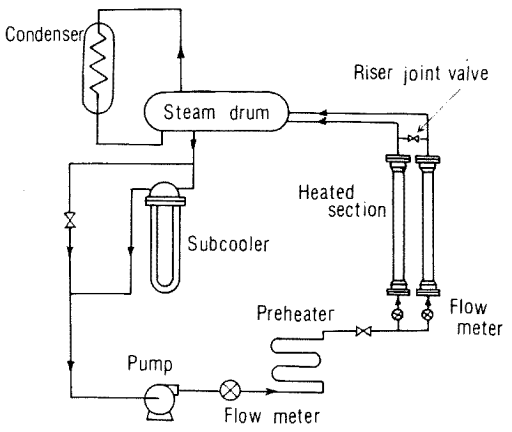

Fig. 1 Flow diagram of heat transfer loop

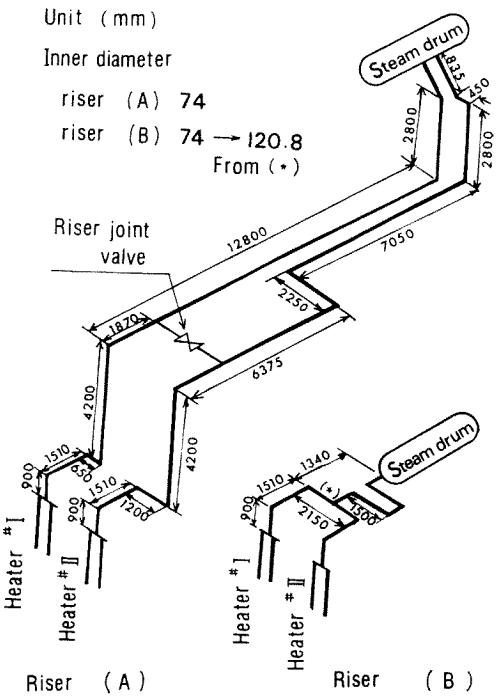

Fig. 2 Configuration of riser pipings

conditions were as follows (**Table 1**) :

Table 1 Ranges of experimental parameters

Test fluid	Water
System pressure P	1~70 kg/cm²·abs
Inlet subcooling ΔT_{SUB}	0~50°C
Channel heating power Q	0~3.2 MW
Inlet throttling (for natural circulation tests) $K \equiv \Delta P/(\frac{1}{2}\rho V^2)$	40~800
Total flow rate W	0.5~17 kg/s

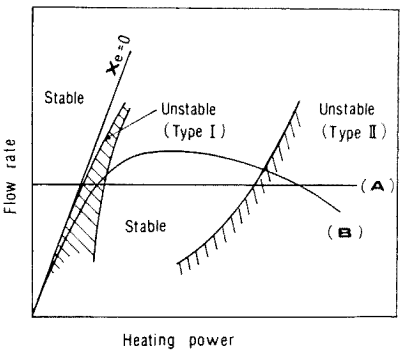

Fig. 3 Comparison between natural circulation and forced circulation

2. Results

Most of the experimental results were shown in our previous paper[7], some of the data being reproduced here. It is shown that both of the data presented here and in the Ref. (7) indicate the existance of two types of instabilities and their characteristic features.

(1) Types of Instabilities

(a) Observations of two types of instabilities: A conceptual stability map is drawn as shown in **Fig. 3,** in which the flow rate curve for both forced (curve A) and natural circulation (curve B) are shown. Under natural circulation, the channel flow rate increases according to the zero-exit-steam-quality-curve as the heating power increases. When the system pressure is low and/or inlet subcooling is high, the flow is unstable at this initial stage. Then the flow rate deviates from the zero-exit-steam-quality-curve and decreases. Usually the flow is stable at this stage, but becomes unstable again when the heating power is increased further. The total flow rate also follows a similar trend, except that the instability regions are narrower than that for the channel flow. Curve A for forced circulation in Fig. 3 shows that there are also two unstable regions; *viz.* the nearly zero steam quality region and the high heating power region. These two regions, termed temporarily Types I and II were clearly observed throughout the experiments. These classifications are made only from the phenomenological point of view, however both types of instability can be predicted by a density wave oscillation model, as is discussed later.

(b) Mode of flow oscillation: There observed two essential modes of oscillation in the natural circulation experiment. One mode is so-called U-tube oscillation characterized by the oscillations of channel flow rates with 180° phase difference. Another mode is the oscillation of channel flow rates in phase each other. In the latter case, total flow rate oscillates in phase with channel flow rate oscillations having an amplitude as large as two times of that of channel flow.

In forced circulation tests only the pure "U-tube" oscillation appears because the total flow rate is kept to a constant value. In natural circulation tests flow oscillation appears sometimes in compound forms of these two extreme modes *e.g.* the "U-tube" oscillation accompanied by total flow oscillation. **Figure 4** (a) and (b) show typical Type I oscillation under natural circulation and forced circulation conditions. It can be seen from Fig. 4(a) that the period of total flow oscillation is exactly half of that of channel flow oscillation. **Figure 5** shows a typical Type II oscillation.

It has been found that the period of oscillation becomes shorter as heating power

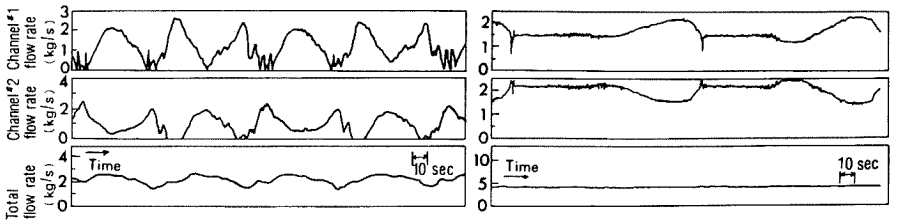

P=1 ata, $\Delta TSUB$=50°C, Q=400 kW (a) Natural circulation

P=1 ata, $\Delta TSUB$=39°C, Q=415 kW (b) Forced circulation

Fig. 4 Typical Type I oscillation under natural circulation and forced circulation conditions

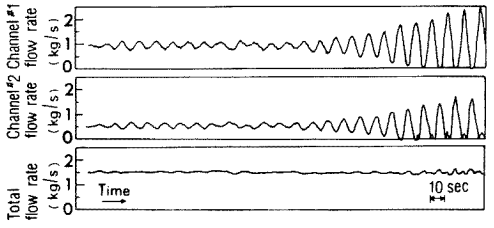

P=1 ata, $\Delta TSUB$=11°C, Q=560 kW

Fig. 5 Typical Type II oscillation under forced circulation

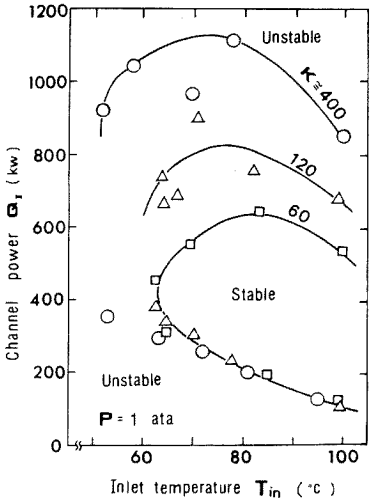

Fig. 6 Stability map showing effect of inlet throttling under natural circulation in test loop with riser (A)

and/or system pressure increases if inlet subcooling or other conditions are fixed. The amplitude of oscillation becomes smaller as system pressure and/or total flow rate increases in forced circulation tests.

(c) Stability map: It is sometimes difficult to discriminate whether an oscillation is "unstable" or "stable". Total flow rate in Fig. 4(a), for example, causes a problem in discrimination. In this paper, "unstable" oscillation is defined as the periodic oscillation or the oscillation with amplitude greater than 30% of average flow rate.

Typical stability map is drawn in **Fig. 6** showing the effect of inlet throttling. Two types of unstable regions are clearly shown in the figure; Type I unstable region lies in low steam quality ($x_e \cong 0 \sim 10\%$) region and Type II in high steam quality ($x_e \gtrsim 30\%$) region. Figure 6 also shows that the inlet throttling has the stabilizing effect, however, this is mostly due to the shift of Type II instability boundary to higher heating power side and there is no change in the Type I boundary. Similar trend was observed in the previous paper[7] regarding the system pressure and inlet flow rate effects.

(2) Effect of Riser

It was observed that the flow became more stable in the Type I unstable region when the riser joint valve (Fig. 2) was opened than when this valve was shut. Opening the valve may equalize the pressure at both side of the valve which would behave as if the riser length were shorter. **Figure 7** shows that the amplitude of channel flow oscillation becomes smaller and the period becomes shorter as the valve is opened. Consequently, it

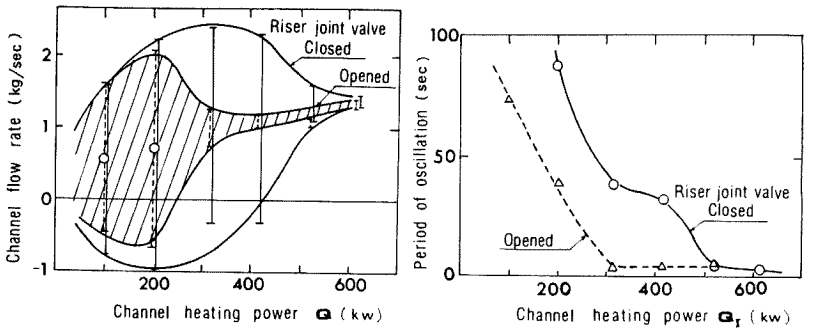

P=10 ata, ΔT_{SUB}=54°C
Effect of riser joint valve to stabilize oscillation of flow rate
Fig. 7

is assumed that the flow becomes more stable as the riser length becomes shorter.

Straightforward evidence of this assumption is obtained by additional experiments which were performed under forced circulation condition using the riser (B) described in Sec. II-1. Typical stability map is drawn in **Fig.** 8 where it can be seen worth noting result that the Type I instability has completely disappeared.

These results could be explained as follows: A small perturbation in flow rate or a consequent perturbation in steam void fraction induces a large change of static pressure drop in the riser or the driving force, and then the change of flow rate. This feed back effect, which is distinguished near a condition $x_e \cong 0$ because of the steep slope of quality *vs.* steam void fraction curve, causes the Type I instability. Then it is realized that the Type I instability is more easily generated in the tests using longer riser pipings.

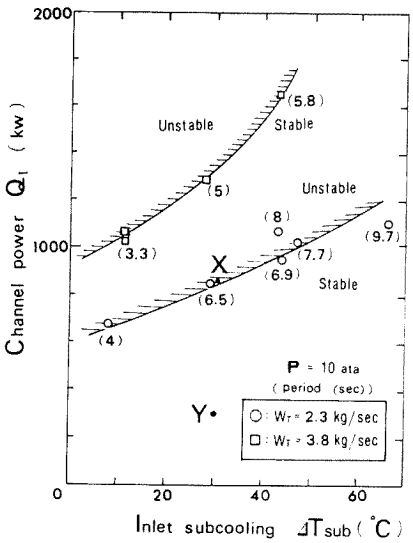

Fig. 8 Stability map under forced circulation test in loop with riser (B)

In the Type II unstable region, however, the frictional pressure drop in the heated section as well as in the riser section plays a dominant role, so the effect of riser length on the Type II unstable region is smaller compared with that on the Type I region.

In the following chapters an analysis will be made and a method is proposed for the classification of instabilities. It will be shown that these two "Types" of instabilities are only a portion of at least eight types of instabilities.

III. ANALYSIS

1. Derivation of Loop Transfer Function

The method of dynamic analysis is used here to investigate into the problem. This method, first adopted by Wallis[6], Jones[8], Davies[9] and by Lahey[10] recently, consists of linearlizing the equations of conservation laws and their Laplace transformations to obtain loop transfer function G in the complex 's' plane.

The assumptions used in the analysis to simplify the problem are as follows:

(1) Physical properties are assumed to be constant.

(2) A term of $\partial P/\partial t$ in energy conservation equation is neglected.

(3) Frictional pressure drop of two-phase flow is given by Eq. (12).
(4) Distribution of heat generation in the test section is uniform.
(5) Heat capacities of the pipings and heated sections are neglected.
(6) Homogeneous flow model is assumed.
(7) Subcooled boiling is neglected.

Errors might be generated by the use of Assumptions (1) and (6) especially at low pressure, however, these assumptions are often applied because of the simplicity of the analysis and convenience of the consequent results for the physical insight into the mechanism of instability.

The analytical procedure is essentially the same to that for well-known "density wave oscillation" analysis[10], so only the outline is described here.

The conservation laws of mass, energy and momentum for the two-phase flow are written by Eqs. (1)~(3).

$$\partial\rho/\partial t+\partial M/\partial z=0\,, \tag{1}$$

$$\frac{\partial}{\partial t}\{\rho_g h_g\alpha+\rho_l h_l(1-\alpha)\}+\frac{\partial}{\partial z}\{\rho_g h_g\alpha V_g+\rho_l h_l(1-\alpha)V_l\}=q'''\,, \tag{2}$$

$$\frac{\partial M}{\partial t}+\frac{\partial}{\partial z}\{\rho_g\alpha V_g{}^2+\rho_l(1-\alpha)V_l{}^2\}+\rho g\sin\theta+\frac{\partial P}{\partial z}+R(z)=0\,, \tag{3}$$

where ρ and M are defined by Eqs. (4) and (5)

$$\rho\equiv\rho_g\alpha+\rho_l(1-\alpha)\,, \tag{4}$$

$$M\equiv\rho_g\alpha V_g+\rho_l(1-\alpha)V_l\,. \tag{5}$$

From Eqs. (1)~(5) we can easily obtain average volumetric velocity V as Eq. (6)

$$V=V_i(t)+\beta(L_0-z_B)\,, \tag{6}$$

where V defined by Eq. (7), is often represented by 'j', however, the letter V is used here to avoid a confusion with $j=\sqrt{-1}$

$$V\equiv\alpha V_g+(1-\alpha)V_l\,. \tag{7}$$

Taking small perturbation of above equations from steady state and Laplace transforming them yield the transfer functions G_V and $G_{\rho,e}$:

$$G_V\equiv\delta\hat{V}/\delta\hat{V}_i=1-(1-e^{-\tau s'})/s'\,, \tag{8}$$

$$G_{\rho,e}\equiv\frac{V^2}{\rho_l V_i}\cdot\frac{\delta\hat{\rho}_e}{\delta\hat{V}_i}=v^{1-s'}(1-G_V)+\frac{1-v^{1-s'}}{s'-1}G_V\,, \tag{9}$$

where $\hat{}$ denotes the Laplace transform and homogeneous flow model defined by Eq. (10) is introduced

$$V_g=V_l=V\,. \tag{10}$$

The functions G_v and $G_{\rho,e}$, represent the non-dimensional transfer functions between inlet velocity *vs.* outlet velocity and between inlet velocity *vs.* outlet density respectively, are very important because they appear explicitly in the equations and suggest the mechanism of instability.

Laplace transform of perturbed part of momentum equation (3) from steady state is given by Eq. (11)

$$\rho(s+\beta+2rV)\delta\hat{V}+(g+\beta V+rV^2)\delta\hat{\rho}+(\partial\delta\hat{p}/\partial z)=0\,, \tag{11}$$

where $R=r\rho V^2$. (12)

Integration of Eq. (11) along two-phase region in heated section yields Eq. (13)

$$\frac{H_2(s)}{\rho_l V_i}=\left\{(1+s')\ln v+K_0\left(1-\frac{z_B}{L_0}\right)\right\}G_V+\frac{1}{\beta}\left(\frac{g}{V_i}G_2+\beta G_1+\frac{K_o}{2L_o}V_iG_0\right), \tag{13}$$

where G_n's are defined by Eq. (14)

$$G_n\equiv\frac{v^{2-s'-n}-1}{2-s'-n}+\frac{G_V}{s'-1}\left\{\frac{v^{1-n}-1}{1-n}-\frac{s'}{2-s'-n}(v^{2-s'-n}-1)\right\}, \tag{14}$$

H_2 represents the transfer function between inlet velocity and pressure drop along the two-phase region in the heated section.

Equations (1)~(5) are also available for the unheated riser section except that the heat source term q''' is substituted by zero. Transportation equation of fluid along the riser is directly obtained from Eq. (1) and described by Eq. (15)

$$\rho(t,\,z)=\rho_1(t-\tau_R,\,z_1)\,, \tag{15}$$

or its perturbed and Laplace transformed expression Eq. (16)

$$\delta\hat{\rho}=e^{-\tau_R s}\delta\hat{\rho}_1\,, \tag{16}$$

where $\rho(t,\,z_1)$ represents the average density of fluid particle which passes through the point z_1 at time t, τ_R the time for the particle to travel from z_1 to z. Using Eq. (16) and integration of Eq. (11) give the transfer function H_3 for the riser section as shown by Eq. (17)

$$\frac{H_3}{\rho_l V_i}=\left(\frac{sL_R}{V_e}+K_R\right)G_V+\frac{1}{\beta}\left(\frac{g}{V_e}\Pi_1+\frac{K_R}{2L_R}V_e\Pi_2\right)G_{\rho.e}\,, \tag{17}$$

$$\left.\begin{aligned}
&\text{where}\quad L_R\equiv\sum_{i.\,\text{Riser}}a_i\Delta L_i\,,\qquad K_R\equiv\sum_{i.\,\text{Riser}}K_i\\
&\Pi_1\equiv 1/s'\sum_{i.\,\text{Riser}}a_it_ip_i(s)\,,\qquad \Pi_2\equiv 1/s'\sum_{i.\,\text{Riser}}a_ik_ip_i(s)\\
&p_i\equiv(1-e^{-(\Delta L_i/V_i)s})e^{-\tau_i s}\,,\qquad t_i\equiv\Delta H_i/\Delta L_i\\
&k_i\equiv(\Delta K_i/K_k)(L_R/\Delta L_i)\,,\qquad a_i\equiv A_o/A_i\,,\qquad V_i\equiv a_iV_e
\end{aligned}\right\}. \tag{18}$$

Transfer function $H_1(s)$ for the single phase region can be easily obtained by Eq. (19)

$$\frac{H_1}{\rho_l V_i}=\left\{\frac{L_{SP}+z_B}{V_i}s+\left(K_{SP}+K_0\frac{z_B}{L_0}\right)\right\}, \tag{19}$$

where $L_{SP}\equiv\sum_{i.\,SP}a_i\Delta L_i$.

A summation of H_i's gives the loop transfer function G or the transfer function between pressure drop along the whole loop and heated section inlet velocity

$$G(s)=\oint(\partial\delta\hat{P}/\partial z)dz/\partial\hat{V}_i=H_1(s)+H_2(s)+H_3(s)\,. \tag{20}$$

Equation (20) which describes the relation between whole loop pressure drop and flow

rate, is a governing equation for studying the hydrodynamic instability problem. From control theory it is known that the flow rate becomes unstable if any one of the loots of Eq. (21) has a positive real part. That is, the flow rate is unstable if Eq. (22) is satisfied

$$G(s_0)=0\,, \tag{21}$$

$$\text{Real part of } s_0>0\,. \tag{22}$$

2. Examination of Basic Transfer Functions

Each of basic transfer functions G_v, $G_{\rho,e}$, G_i $(i=0,1,2)$ or Π_i $(i=1,2)$ is examined in this section to survey its role in the instability characteristics. The usual procedure is followed, that is, the Laplace transform variable s is replaced by $j\Omega$, then Ω is changed from $-\infty$ to ∞ to plot the Nyquist diagram. Typical Nyquist diagrams for the basic transfer functions are shown in **Fig. 9.**

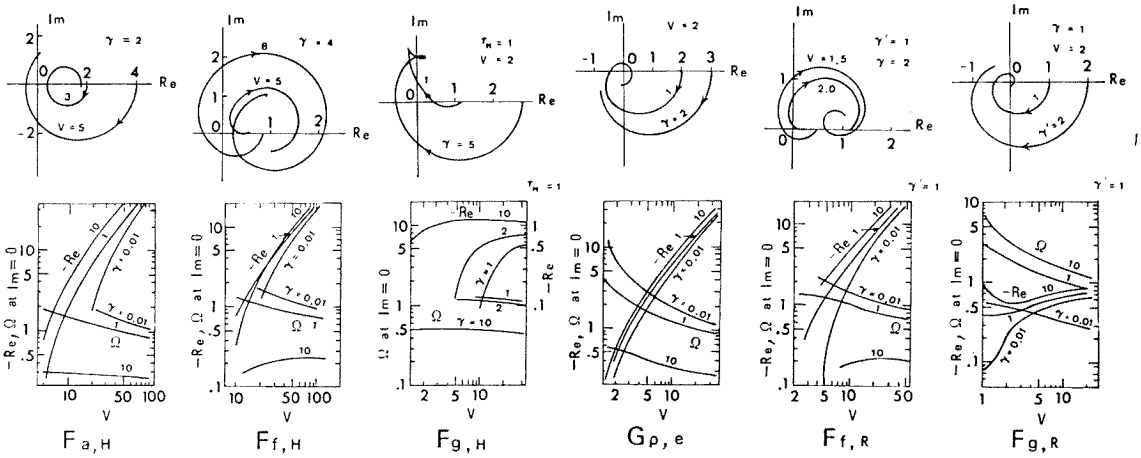

Fig. 9 Nyquist diagram of major transfer functions F's and Ω or Re at $\angle F=\pi$

$G_V(s)$: $G_V(j\Omega)$ has the static characteristics that if $\gamma>1$, $G_V(j\Omega)|_{\Omega\to 0}=1-\gamma<0$, which implies that the increase (or decrease) of inlet flow rate results in the decrease (or increase) of outlet flow rate as $t\to\infty$. This characteristics can cause the Ledinegg instability as is shown later.

$G_{\rho,e}(s)$: Nyquist diagram of $G_{\rho,e}(j\Omega)$ turns around the origin for every γ and v and can cause the instability. Two limits of $G_{\rho,e}$ are given by Eqs. (23) and (24)

$$G_{\rho,e}|_{s'\to 0}=v+\gamma-1>0\,, \tag{23}$$

$$G_{\rho,e}|_{v\to\infty}=v/(1-s')e^{-s'(\gamma+\ln v)}\,. \tag{24}$$

Equation (23) implies that $G_{\rho,e}$ is not the cause of the static instability but the dynamic one or the so-called density wave type instability. It is also found that the instability related to $G_{\rho,e}$ is easier to be generated for larger v because the magnitude of $G_{\rho,e}$ is of the order v, as is shown by Eq. (24). This trend corresponds to the experimental result that the instability occurs at rather high steam quality as the heating power is increased keeping other parameters (system pressure, inlet flow rate, inlet temperature and so on) constant.

$\boldsymbol{G_i(s)}$ $\boldsymbol{(i=0, 1, 2)}$: G_i's are the transfer functions between inlet velocity and frictional pressure drop $(i=0)$, or momentum pressure drop $(i=1)$, or gravity in the heated section $(i=2)$. From drawing the Nyquist diagram it is found that the G_0 and G_1 can cause the instability. On the contrary, the term G_2 itself is stable although, it can cause the dynamic instability in combination with the acceleration term as shown by Eq. (25).

As the magnitude of G_i is $O(v^2)$ $(i=0)$, $O(v)$ $(i=1)$ and $O(1)$ $(i=2)$, the friction term $(i=0)$ becomes more dominant as v increases.

It is found that G_0 and G_1 always appear in proper combination with G_V as shown by Eqs. (26) and (27) respectively,

$$F_{g.H} \equiv G_2 + (V_i \tau_{SP} \beta / g) s \,, \tag{25}$$

$$F_{f.H} \equiv (1-P_B) G_V + (1/2)(P_B/\gamma) G_0 + P_B \,, \tag{26}$$

$$F_{a.H} = \ln v \cdot G_V + G_1 \,. \tag{27}$$

The major characteristics of Eqs. (25)~(27) are shown in Fig. 9.

$\boldsymbol{\Pi_i G_{\rho.e}}$ $\boldsymbol{(i=1, 2)}$: Transfer functions related to the transportation of the fluid particle in the unheated riser section. Π_i takes the form:

$$\Pi_i = c \int_0^{L_R} \delta\hat{\rho}\, dz / \delta\hat{\rho}_e \,, \tag{28}$$

where integration should be made along the vertical section for $i=1$ and along the whole length for $i=2$. Although Π_i itself is not unstable the product of Π_i and $G_{\rho.e}$ becomes unstable because of the unstable characteristics of $G_{\rho.e}$.

If the riser consists of single vertical pipe, Π_i is given by Eq. (29)

$$\Pi_i = (1 - e^{-i' s'}) / s' \,. \tag{29}$$

Π_i advances the phase of $G_{\rho.e}$ and this effect becomes larger as γ' increases. In other words, the period of riser dominant unstable flow oscillation becomes longer if the longer riser pipe is used.

The gravity term is always unstable because it appears in the form of $\Pi_1 G_{\rho.e}$, however the friction term takes the form of the combination with G_V as Eq. (30), and has the stable region

$$F_{f.R} \equiv G_V + (1/2)(\Pi_2/\gamma') G_{\rho.e} \,. \tag{30}$$

3. Density Wave Instability and Ledinegg Instability

(1) Density Wave Instability[10]

From the above analysis it is concluded that G_0 (or $F_{f.H}$), G_1 (or $F_{a.H}$) and $\Pi_i G_{\rho.e}$ (or $F_{f.R}$ for $i=2$) can cause the instability. G_2 also can cause instability if it is combined with the acceleration term. The instability, in which one (or more) of these terms plays the governing role, may correspond to the so-called density-wave instability. The period should be the magnitude of the order τ of τ_R. $G_{\rho.e}$, for example, has the term $v^{-j\Omega} = e^{-j\tau\omega}$ predicts the period of order τ because the frequency at $\angle G_{\rho.e} = \pi$ is approximately equals $\omega = O(\pi/\tau)$. This prediction coincides with the experimental observation on the density wave oscillation that its period is the order of the transit time for the fluid particle

through the two-phase region. More exact value of Ω is calculated for each basic transfer function F and shown in Fig. 9.

Stability maps for $F_{f.H}$, $F_{f.R}$, $F_{a.H}$ and $F_{g.H}$ are drawn in **Fig. 10**(a)~(c). Consulting Fig. 9 together with Fig. 10 (a)~(c), it can be concluded that the instability due to some of these terms inevitably occurrs if v, or heating power, is increased unlimitedly because the gain $|F|$ at $\angle F=\pi$ increases to surpass other stabilizing terms.

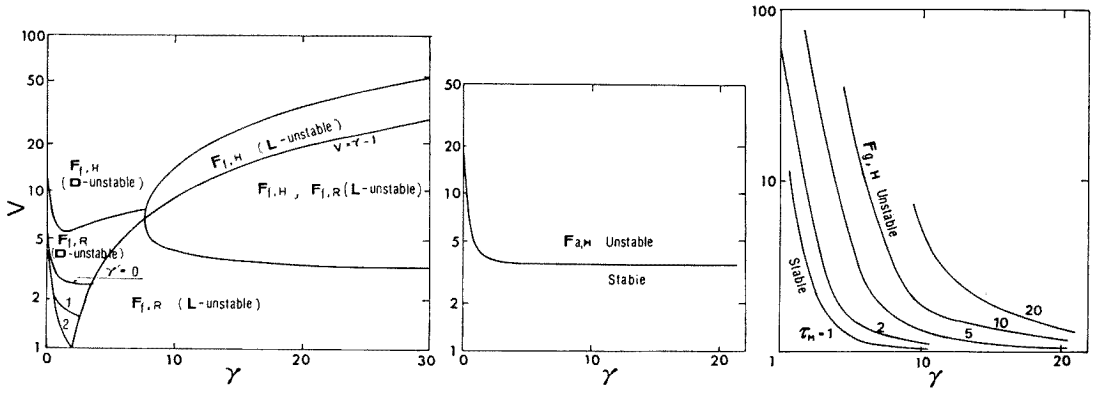

(a) D_{II}, L_I, L_{II} type instabilities (b) D_{III} type instability (c) $D_{I,H}$ type instability

Fig. 10 Analytically derived stability maps

(2) Ledinegg Instability

The Ledinegg instability[11] is attributed to the negative slope on the loop pressure drop ΔP *vs.* flow rate curve, the criterion being written by Eq. (31)

$$\partial \Delta P/\partial V_i<0\,, \tag{31}$$

where ΔP is given by Eq. (32)

$$\Delta P=\oint(\rho(DV/Dt)+\rho g\sin\theta+R(z))dz\,. \tag{32}$$

By a straightforward but rather complicated calculation we can get Eq. (33).

$$\frac{\partial \Delta P}{\partial V_i}=\rho_l V_i\Big[v-1+\frac{g}{\beta V_i}\Big[\ln v+(\gamma-1)(1-v^{-1})+\beta\frac{H_R}{V_e}\Big(1+\frac{\gamma-1}{v}\Big)\Big]$$
$$+\Big[K_{SP}+K_o P_B\Big\{\frac{(v-1)}{4\gamma}+\Big(\frac{1}{\gamma}-\frac{1}{2}\Big)(v-1)+1\Big\}+K_R\frac{1+v-\gamma}{2}\Big]\Big]\,, \tag{33}$$

where $P_B=z_B/L_0=\tau_B/\tau_0=\gamma/(\gamma+v-1)$.

It is easily shown that the Eq. (33) can be derived also by Eq. (34)

$$\partial \Delta P/\partial V_i=G(s)|_{s\to 0}\,. \tag{34}$$

This coincidence is reasonable because the limit $G(s)|_{s\to 0}$ is equivalent to $\lim_{s\to 0}(\widehat{\delta P}/\widehat{\delta V_i})$ or $\lim_{t\to\infty}(\delta P/\delta V_i)$.

It is found from Eq. (33) that the Ledinegg instability is only arised from the terms of frictional pressure drop in the heated section and the riser. The range, in which these terms have the negative slope characteristics on the ΔP *vs.* V_i curve, can be obtained by Eqs. (35) and (37), and shown in Fig. 10(a).

$$v_1<v<v_2 \quad \text{for heated section}\,, \tag{35}$$

where

$$v_i \equiv 2\gamma\left\{\left(\frac{1}{2}-\frac{1}{\gamma}\right) \pm \sqrt{\left(\frac{1}{\gamma}-\frac{1}{2}\right)^2-\frac{1}{\gamma}}\right\}+1 \qquad (i=1, 2)\ , \tag{36}$$

$$v<\gamma-1 \quad \text{for riser.} \tag{37}$$

From the figure, the rough criteria for the Ledinegg instability could be obtained as follows; the Ledinegg instability due to the frictional pressure drop in the heated section does not occur if (i) $\gamma \leqq 2(2+\sqrt{3})=7.46$, (ii) $v \leqq 3$, (iii) $P_B \leqq 1/3$ and the Ledinegg instability due to the frictional pressure drop in the riser section does not occur if (i) $\gamma \leqq 2$, (ii) $P_B \leqq 1/2$.

From the derivation of Eq. (34) it is known that $G_V(s)|_{s\to 0}$ should be at least negative for the Ledinegg instability to arise. This correspond to the phenomenologicaly important trend that at the Ledinegg instability condition the outlet velocity increases (or decreases) as inlet velocity decreases (or increases) keeping other parameters constant, or described by equation: $\partial V_e/\partial V_i<0$.

4. Classification of Instabilities

The analysis shown in Sec. Ⅲ-3 is summarized in **Table 2** where each governing parameter represents the product of magnitude of a transfer function and its coefficient, showing the importance of its term. It is shown that so-called hydrodynamic instability of the two-phase flow in a loop might be classified into three types of Ledinegg instabilities and five types of density wave instabilities, in each type different pressure drop term plays an dominant role. Types $D_{\mathrm{I},H}$, $D_{\mathrm{I},R}$ and L_{I} shown in Table 2 are easily created even if the low steam quality condition or $v \cong 1$, while the types $D_{\mathrm{II},H}$, $D_{\mathrm{II},R}$ and L_{II} occurs in high quality condition. The conditions for the types D_{III} and L_{III} are rather peculiar such as that the effect of friction and/or gravity is negligibly small. The Types I and II mentioned in Chap. II might correspond to the types $D_{\mathrm{I},R}$ and $D_{\mathrm{II},H}+D_{\mathrm{II},R}$ respectively.

This kind of classification is convenient to know the cause of instability and to take

Table 2 Classification table for hydrodynamic instabilities

Equation	Coefficient	Magnitude at $s\to 0$	Type†	Contents	Representative period	Unstable region
$F_i=s\tau_{TP}G_V$	1	N_2	L_{III}	Inertia of two-phase fluid	τ_B	$\gamma>1$
$F_{a,H}=G_1+\ln v\cdot G_V$	1	N_1	D_{III}	Acceleration in heated section	(τ_B), τ_o	Fig. 10(b)
$F^L_{f,H}=(1-P_B)G_V+P_B$	K_o	K_oN_4	L_{II}	Friction in heated section	(τ_B)	Fig. 10(a)
$F^D_{f,H}=(1/2)(P_B/\gamma)G_0$	K_o	K_oN_1	$D_{\mathrm{II},H}$		(τ_B), τ_o	
$F^L_{f,R}=G_V$	K_R	K_RN_2	L_{I}	Friction in riser section	(τ_B)	Fig. 10(a)
$F^D_{f,R}=(1/2)(\Pi_2/\beta\tau_R)G_{\rho,e}$	K_R	K_RN_3	$D_{\mathrm{II},R}$		(τ_B), τ_o, τ_R	
$F_{g,H}=G_2+(V_i\tau'_{sp}\beta/g)s$	$g/\beta V_i$	gH/V_i^2	$D_{\mathrm{I},H}$	Gravity in heated section and inertia of-sigle phase fluid	(τ_B), τ_o	Fig. 10(c)
$F_{g,R}=(1/v)\Pi_1G_{\rho,e}$	$g/\beta V_i$	$(gH_R/V_i^2)N_5$	$D_{\mathrm{I},R}$	Gravity in riser section	(τ_B), τ_o, τ_R	Unstable for every (v, γ, γ')

(†) D: Density wave instability, L: Ledinegg instability

$N_1=v-1$, $N_2=1-\gamma$, $N_3=v+\gamma-1=N_1-N_2+1$, $N_4=1-\gamma+\gamma^2/(v+\gamma-1)=N_2+\gamma^2/N_3$

$N_5=(v+\gamma-1)/v^2=N_3/v^2$, $\tau_{TP}=\tau_0+\tau_R$, $\tau'_{PS}=\tau_{SP}+\tau_B$, $\tau_M=V_i\tau'_{SP}\beta/g$

adequate preventive measure against the instability. The procedure to know what type(s) are the experimentally observed instabilities classified into is as follows:

(1) First calculate each governing parameters to know the largest one.

(2) Then check if the corresponding type of instability can be be generated by consulting its stability map. If not, same procedure should be repeated from (1).

(3) If more than one governing parameters are of the almost same magnitude then the type of longer representative time is considered to be more dominant.

5. Application of Analysis to Experimental Data

The method for the classification of instabilities described in Sec. III-4 is applied to some of our data and Masini's[12].

Dimensions of the loop, conditions for calculation and the results are listed in **Table 3.**

It is found that typical instabilities for the loop with long risers (A) presented in Figs. 4(b) and 5 are clearly classified into the type $D_{\mathrm{I},R}$ and $D_{\mathrm{II},H}$ respectively. And that the

Table 3 Classification of various experimentally observed instabilities

Reference		Present Paper				Masini[10]
Figure or Table		Fig. 4(b)	Fig. 5	Fig. 8(X)	Fig. 8(Y)	Table 2
Stable or unstable		Unstable	Unstable	Unstable	Stable	Unstable
Period	(s)	115	10.5	6.5	—	—
L_{SP}	(m)	9.825		9.825		1.47
L_o	(m)	5.3		5.3		3.0
H_o	(m)	5.3		5.3		3.0
L_R	(m)	22.96		4.91		4.39
H_R	(m)	8.735		0.		5.94
K_o	(—)	33.2		33.2		12.0
K_R	(—)	12.0		1.8		5.07
ρ_{lg}/ρ_g	(—)	850.0	850.0	147.8	174.8	30.4
V_i	(m/s)	0.427	0.107	0.267	0.267	0.233
Δx_{SUB}	(—)	0.072	0.020	0.06	0.06	0.098
x_e	(—)	0.	0.476	0.33	0.01	0.119
τ_B	(s)	11.6	2.0	3.1	17.	5.8
τ	(s)	0.	0.7	1.2	1.6	3.0
τ_R	(s)	54.	0.53	0.3	6.7	4.1
τ_M	(s)	8.0	8.7	3.7	0.9	0.1
v	(—)	1.	405.6	58.7	2.8	4.6
γ	(—)	61.2	17.0	10.5	10.5	3.0
γ'	(—)	265	4.5	1.1	4.1	2.1
L_{I}	(—)	−722.0	−192.0	−17	−17	−10
$D_{\mathrm{I},H}$	(—)	285.0	4536	729	729	541
$D_{\mathrm{I},R}$	(—)	28,728.	19.2	0	0.2	332
L_{II}	(—)	33	−508.0	−261	−16.5	−7.6
$D_{\mathrm{II},H}$	(—)	0.	13432	1915	58	43
$D_{\mathrm{II},R}$	(—)	734.0	5059	123	22	33
L_{III}	(—)	−36.	0.8	0.6	−0.4	−0.1
D_{III}	(—)	0.	405	58	2	3.6
Type of instability		$D_{\mathrm{I},R}$	$D_{\mathrm{II},H}$	$D_{\mathrm{II},H}$	$(D_{\mathrm{I},H})$	$D_{\mathrm{I},R}$, $D_{\mathrm{I},H}$

instability data for the loop with short risers (B) denoted by the point X in Fig. 8 is classified into $D_{\mathrm{II}.H}$. While at the point Y, where the flow rate was stable, $D_{\mathrm{I}.H}$ is found to be the governing term and the $D_{\mathrm{I}.R}$ type instability diminishes. However, it is necessary to calculate whole loop transfer function G exactly to know whether $D_{\mathrm{I}.H}$ type instability occurs or not.

One of the data of instability obtained by Masini[12] is also examined and classified into the type $D_{\mathrm{I}.R}$.

IV. Conclusion

Hydrodynamic instabilities of two-phase flow could be classified into at least eight types of instabilities, where different pressure drop term : gravitational, frictional pressure drop *etc.* plays a dominant role in each type.

Three of them are classified into so-called Ledinegg instability and five are into the density wave instability.

Classifications presented in this paper is convenient to know the cause of instability and to apply for the technical purpose such as to take adequate preventive measure against the instability.

Two typical types of instabilities have been observed in our experiment and classified according to the classification procedure proposed in this paper.

[Nomenclature]

F: Transfer function defined by Eqs. (25)～(27), (30)
g: Acceleration of gravity = 9.81 m/s^2
G: Transfer function defined by Eqs. (8), (9), (14), (20)
h: Enthalpy (kcal/kg)
h_{gl}: Latent heat (kcal/kg)
Δh_{SUB}: Inlet subcooling (kcal/kg)
H_i: Transfer function defined by Eqs. (13), (17), (19)
H_R: Height of riser piping (m)
K: Friction factor defined by $\Delta P/(\rho_l V_i^2/2g)$
L: Length (m)
ΔL: Length of segment of piping (m)
M: Momentum defined by Eq. (5) (kg/m^2·s)
P: Pressure (kg$_f$/m^2)
$P_B = z_B/L_0$
ΔP: Pressure drop (kg$_f$/m^2)
q''': Heat generation rate of heated section per unit volume of fluid (kcal/m^3·s)
R: Frictional pressure drop per unit length (kg$_f$/m^3)
r: Defined by Eq. (12) (1/m)
s: Laplace parameter (1/s)
$s' = s/\beta$
t: Time (s)
$v = V_e/V_i$
V: Volumetric flow velocity (m/s)
x: Steam quality
z: Longitudinal coordinate (m)
z_B: Length from bottom of heated section to point of bulk boiling initiation
α: Void fraction
$\beta = \gamma/\tau_B$ (1/s)
$\gamma = (\rho_{lg}/\rho_g)(\Delta h_{SUB}/h_{gl})$
$\gamma' = \beta\tau_R$
θ: Angle of inclination from horizon (rad)
Π_i: Defined by Eq. (18)
ρ: Density (kg/m^3)
$\rho_{lg} = \rho_l - \rho_g$ (kg/m^3)
τ: Transit time (s)
τ_B: Time required for fluid particle to lose its subcooling z_B/V_i (s)
τ_0: Transit time of fluid particle in two-phase region of heated section $\ln v/\beta$ (s)
ω: Angular velocity (rad/s)
Ω: Nondimensional angular velocity ω/β

Subscripts

e: Exit of heated section
g: Gas
i: Inlet of heated section
l: Liquid
o: Heated section
R: Riser section
SP: Inlet piping section or single phase region

ACKNOWLEDGMENT

The authors wish to express their thanks to the colleagues at the Heat Transfer Laboratory, Power Reactor and Nuclear Fuel Development Corporation, for their contribution to this experiment, Prof. K. Sekoguchi for instructive discussions.

—REFERENCES—

(1) ARITOMI, M., *et al.*: *J. Nucl. Sci. Technol.*, 14[2], 88~96 (1977).
(2) SUZUOKI, A., YAMAKAWA, M.: *Trans. JSME*, (in Japanese), 41[350], 2866~2877 (1975).
(3) SUMIDA, I., KAWAI, T.: *J. Nucl. Sci. Technol.*, 15[5], 323~337 (1978).
(4) BOURE, J.A., *et al.*: *ASME* 71-HT-42, (1971).
(5) HARVIE, J.D.: *Symp. at Univ. of Strathclyde*, Multi-phase flow systems, El, (1974).
(6) WALLIS, G.B., HEASLEY, J.H.: *J. Heat Transfer*, 83C, 363~369 (1961).
(7) FUKUDA, K., KOBORI, T.: *6th Int. Heat Transfer Conf.*, FB-17, (1978).
(8) JONES, A.B.: *KAPL*-2170, (1961).
(9) DAVIES, A.L., POTTER, R.: *Symp. on Two Phase Flow Dynamics, Eindhoven*, 9.3, (1967).
(10) LAHEY, Jr. R.T., YADIGAROGLU, G.: *5th Int. Heat Transfer Conf.*, B5.9, (1974).
(11) LEGINEGG, M.: *Die Wärme*, (48), 891~898 (1938).
(12) MASINI, G., *et al.*: *Energ. Nucl.* 15[12], 777~786 (1968).

Errata (Vol. 16, No. 1 (1979))

Page	Line	As printed	To read
33	Eq. (7)	$\left(\frac{d\gamma}{dP}\right)_s=\frac{q}{a^2}$.	$\left(\frac{d\gamma}{dP}\right)_s=\frac{g}{a^2}$.
36	Eq. (33)	$V_G=\pi\{rx\ddot{x}+\dot{x}(r\dot{x}+\dot{r}x)\}$.	$\dot{V}_G=\pi\{rx\ddot{x}+\dot{x}(r\dot{x}+\dot{r}x)\}$.
37	Eq. (41)	$u(y_0)A_G(y_0)=\pi_0^2 y\dot{x}$.	$u(y_0)A_G(y_0)=\pi y_0^2\dot{x}$.
38	15	$\dot{x}$, T_L and $\ddot{l}_H$ are ·····	$\dot{x}$, $\dot{T}_L$ and $\ddot{l}_H$ are ·····
42	[NOMENCLATURE]		
	Right column 13	W_0: Steam flow rate ···	W_0: Steam flow rate ···
〃	〃 26	ξ: Flow coefficient (≒0.65)	ζ: Flow coefficient (≒0.65)
〃	Left column 15	g: Gravitational acceleration	g: Gravitational acceleration
39	Add to end of **Table 1** further values: $\zeta=0.65$, $\xi=0.5$, $l_v=5.03$ m.		